Langmuir

Article

pubs.acs.org/Langmuir

Electrostatic Stabilization of Graphene in Organic Dispersions

Andrew N. J. Rodgers, Matěj Velický, and Robert A. W. Dryfe*

School of Chemistry, University of Manchester, Oxford Road, Manchester M13 9PL, United Kingdom

Supporting Information

ABSTRACT: The exfoliation of graphite to give graphene dispersions in nonaqueous solvents is an important area with regards to scalable production of graphene in bulk quantities and its ultimate application in devices. Understanding the mechanisms governing the stability of these dispersions is therefore of both scientific interest and technological importance. Herein, we have used addition of an indifferent electrolyte to perturb few-layer graphene dispersions in a nonaqueous solvent (1,2-dichloroethane) as a way to probe the importance of interparticle electrostatic repulsions toward the overall dispersion stability. At a sufficient electrolyte concentration, complete sedimentation of the dispersions occurred over 24 h, and the relationship between dispersed graphene concentration and electrolyte concentration was consistent with a dispersion stabilized by electrostatic repulsions. We also found that an increased oxygen content in the graphite starting material produced dispersions of greater stability, indicating that the extent of oxidation is an important parameter in determining the extent of electrostatic stabilization in nonaqueous graphene dispersions.

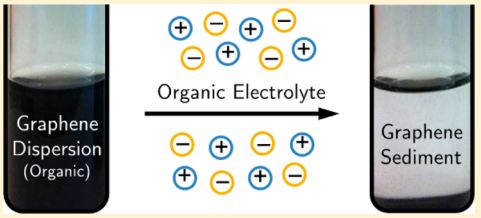

INTRODUCTION

Since it was first isolated a decade ago,[1,2] the unique properties of graphene and its potential applications have sparked an enormous amount of research. Of key importance in the realization of graphene's full potential is the development of scalable bulk production methods. This has led to much work on nonaqueous solvent exfoliation of graphite to give graphene dispersions as a promising procedure for inexpensive production of graphene in bulk quantities.[3−6] *N*-Methyl-2-pyrrolidone (NMP), dimethyl sulfoxide (DMSO) and *N*,*N*-dimethylformamide (DMF) are regarded as among the best solvents for this procedure. Because of its hydrophobic nature, pristine graphene does not disperse well in water, though aqueous dispersion can be achieved by functionalization with surfactants[7,8] or oxidation to graphene oxide (GO).[9,10] GO and reduced GO (rGO) have also been successfully dispersed in certain nonaqueous solvents.[11−14]

It is generally acknowledged that these nonaqueous graphene dispersions are thermodynamically unstable due to strong intersheet van der Waals (vdWs) attractive forces and will eventually aggregate and sediment out of dispersion.[5,15,16] Such dispersions are termed lyophobic colloids and often described by the theory of Derjaguin, Landau, Verwey, and Overbeek (DLVO).[17]

There has been a considerable amount of work aimed at maximizing the extent of exfoliation, flake size, and dispersion concentration of nonaqueous graphene dispersions,[18−20] with thermodynamics used to rationalize which solvents are the best. The Gibbs energy of mixing a species and solvent per unit volume (ΔG_{mix}) is given by eq 1, where T is temperature and ΔH_{mix} and ΔS_{mix} are the enthalpy and entropy, respectively, of mixing per unit volume. ΔS_{mix} will be positive, although small, for a rigid structure like graphene.

$$\Delta G_{mix} = \Delta H_{mix} - T\Delta S_{mix} \quad (1)$$

It is thought, therefore that "good" solvents must minimize the enthalpic cost of mixing, and in turn the thermodynamic instability of these dispersions, by having a similar surface energy to graphene.[5] Through modeling experimental dispersed graphene concentrations in a range of solvents with differing surface energies, the surface energy of graphene was estimated to be ca. 68 mJ m^{-2}. This analysis was subsequently expanded to matching the Hildebrand and Hansen solubility parameters of solvent and graphene.[21]

Despite their thermodynamic instability, graphene dispersions in certain nonaqueous solvents have been reported to show very good kinetic stability toward aggregation and sedimentation over a period of months.[3,20] However, there have been relatively few in-depth studies probing the this kinetic stability, which is surprising, given that a full understanding of the mechanisms governing the kinetic stability of nonaqueous graphene dispersions is essential for their incorporation in many practical applications.

In the DLVO theory of lyophobic colloids, there are two principal repulsive forces which can counteract attractive interparticle forces (vdWs in the case of graphene) and, if sufficient in magnitude, render dispersions stable for an extended period of time.[17,22,23] These are (1) electrostatic, where the presence of surface charge establishes an electrical double layer (EDL) around the colloidal particles and results in an electrostatic repulsion between approaching particles, and (2) steric, where bulky surface groups physically prevent the close approach of particles.[22] It is important to realize that any discussion of stability with respect to lyophobic colloids is of a

Received: March 5, 2015
Published: November 17, 2015

DOI: 10.1021/acs.langmuir.5b04219
Langmuir 2015, 31, 13068−13076

purely kinetic nature, and all lyophobic colloids will eventually aggregate and sediment out. The repulsive forces simply provide an energetic barrier to aggregation.

Molecular dynamics (MD) simulations by Shih et al.[24] and Fu and Yang[25] have highlighted the importance of a structured layer of solvent molecules which forms around the surface of dispersed graphene sheets and provides a steric barrier to aggregation, thus opposing the vdWs attraction and aiding dispersion stability. Thus far, there has been an (almost total) absence of studies probing the contribution of surface charging to the stabilization of unfunctionalized, nonaqueous, graphene dispersions. However, Liu et al.[26] showed, through measurements of zeta potential (ζ), that as-dispersed graphene sheets do possess surface charge in a range of nonaqueous solvents. Indeed, they posited that electrostatic forces were the key factor determining the stability of graphene in nonaqueous dispersion.

The origin of surface charge on pristine graphitic materials in nonaqueous dispersion is generally not well understood. Dispersion in chlorosulfonic acid is an exception, where protonation of the graphene flakes occurs, lending these dispersions great kinetic stability due to electrostatic repulsions.[27] Liu et al.[26] observed a correlation between solvent donor number (DN) and ζ sign, for graphene dispersions, and proposed that surface charge is a result of electron transfer between graphene and the dispersing solvent. It is known that aqueous dispersions of GO possess a negative surface charge due to dissociation of oxygen containing functional groups (in particular, COOH).[10,28−32] Ameen et al.[33] have suggested that the extent of oxidation may also determine the magnitude of surface charge on carbon nanotubes (CNTs) in nonaqueous dispersion. In reality, unfunctionalized graphitic materials are not composed solely of carbon but also contain impurities, with oxygen from the graphite starting material being common. Therefore, it is possible that dissociation of oxygen-containing functional groups may contribute to the charging of nonaqueous graphene dispersions.

One of the most common ways to probe electrostatically stabilized colloids is through the addition of an indifferent electrolyte, which does not directly interact with the surface of the colloidal particles but simply screens their surface charge through the presence of positive and negative ions. These ions compress the EDL around the particles, thus reducing the electrostatic barrier to particle aggregation. The size of the EDL decreases with increasing electrolyte concentration, until eventually it is negligible and particle aggregation is simply controlled by diffusion. The concentration at which this occurs is known as the critical coagulation concentration (CCC). To the best of our knowledge, and despite its clear importance, there is no existing work on the perturbation of nonaqueous graphene dispersions by electrolyte. Several such studies have been performed on aqueous GO dispersions,[10,28−30,34−36] and perhaps the most relevant work to this study is that of the Poler group on electrolyte-induced aggregation of CNT dispersions in NMP and DMF.[33,37−39]

To address these phenomena, we present a study on electrolyte-induced sedimentation of nonaqueous graphene dispersions and demonstrate that this behavior is consistent with that of an electrostatically stabilized colloid. Dispersions were prepared from two graphite powders of differing oxygen content to probe the effect of oxidation extent on the electrostatic stabilization of nonaqueous graphene dispersions. 1,2-Dichloroethane (DCE) and 1,2-dichlorobenzene (DCB) were used as the dispersing media. These solvents were chosen due to their compatibility with the interface between two immiscible electrolyte solutions (ITIES),[40,41] which provides an interesting platform for the study of graphene's interfacial properties and electrochemistry.[42,43] Though not the most commonly used solvents for dispersion of graphitic materials, DCE and DCB have previously been used to disperse graphene,[20,44−46] CNTs,[47−50] and C_{60}.[51] Furthermore, commonly used dispersion media such as NMP and DMF are miscible with water and therefore not suitable for studies of adsorption at the organic/water interface or at the ITIES.

EXPERIMENTAL PROCEDURE

Materials. DCE (Chromasolv, ≥99.8%) and DCB (Chromasolv, 99%) were used as purchased. The organic electrolyte, bis(triphenylphosphoranylidene)ammonium tetrakis(4-chlorophenyl)borate (BTPPATPBCl, see Supporting Information, Figure S1, for structure), was prepared by metathesis of BTPPACl (97%) and KTPBCl (≥98%), as described in the literature.[52] A slight variation in procedure was adopted, with a 2:1:1 acetone:ethanol:water mixture used here for the initial metathesis reaction and a 1:1 acetone:ethanol mixture used for recrystallization. All solvents and chemicals were purchased from Sigma-Aldrich, UK.

Graphite powder, produced from a binder-free graphite rod (GRod), was used for preliminary studies, and two powders produced from different sections of a single larger piece of natural graphite (NG I and NG II) were used for more detailed study. All graphite samples were supplied by Graphexel Ltd. (UK) and the powders prepared by ball-milling.

Preparation of Graphene Dispersions. Graphene dispersions were prepared by adding organic solvent to graphite powder, at an initial concentration of 1000 mg L^{-1}. Unless otherwise stated, the mixture of solvent and graphite was sonicated for 2 h (Elmasonic P 70 H sonic, 70% power, 37 kHz). After sonication, the following procedure, adapted from the work of Coleman et al.,[3,7,18,19,21] was used to remove the larger particles/aggregates. Dispersions were left to stand for 24 h; the supernatant was collected and then centrifuged at 30g (587 rpm) for 45 min (Sigma 2-16 benchtop centrifuge). The resulting supernatant was collected as the final dispersion.

Characterization of Graphene Dispersions. Prior to dispersion, the graphite powders were characterized with X-ray photoelectron spectroscopy (XPS), with each powder pressed into a solid pellet for this analysis. XPS spectra of graphene flakes after dispersion were also recorded, with the dispersions filtered through a poly(vinylidene fluoride) (PVDF) membrane. All XPS measurements were performed on a Thermo Scientific K-Alpha spectrometer, using a monochromatic Al Kα X-ray source (100 W), at the NEXUS facility (Newcastle University, UK). Analysis of XPS data was performed using CasaXPS software, version 2.3.17.

Size distributions of dispersed particles were characterized using dynamic light scattering (DLS), scanning electron microscopy (SEM), and atomic force microscopy (AFM). Raman spectroscopy was used to assess number of graphene layers and extent of defects. Zeta-potential (ζ) measurements were employed to assess the surface charge on dispersed particles.

DLS and ζ measurements were performed *in situ* on a ZetaSizer Nano-ZS (Malvern Instruments) using irradiation from a 633 nm He−Ne laser. DLS measured the hydrodynamic diameter (d_H) of a particle, which is the diameter of a hypothetical perfect sphere diffusing at the same speed as the particle under observation.[53] To determine ζ, electrophoretic mobility (μ) was measured and the Smoluchowski approximation (applicable when the particle radius is significantly larger than the EDL thickness)[7,54] was used to convert μ to ζ.

Samples for SEM, AFM, and Raman measurements were prepared by spin-coating 1 mL of dispersion onto a Si/SiO_2 wafer (1000 rpm for 3 min). An FEI XL30 Environmental FEG scanning electron microscope, operated under high-vacuum mode, was used for SEM measurements. Analysis of SEM images was performed using ImageJ software, with the longest lateral dimension (length) of each particle

DOI: 10.1021/acs.langmuir.5b04219
Langmuir 2015, 31, 13068−13076

measured. The total number of particles measured was 411, 301, and 244 for dispersions of GRod, NG I, and NG II, respectively. AFM measurements were performed on a Multimode 8 atomic force microscope (Bruker, USA), operating in PeakForce tapping mode with an SNL-10 Si-tip on a Si_3N_4 cantilever. Nanoscope software (version 8.15, Bruker, USA) was used to operate the AFM, and SPIP (version 6.3.0, Image Metrology A/S, Denmark) software was used for particle analysis. Height values quoted in this report are the mean particle height, and the length is the longest lateral particle dimension. Raman measurements were performed on an inVia Raman spectrometer (Renishaw, UK) operated at <1 mW power. A 633 nm wavelength laser and 100× objective were used (laser spot size ≈1 μm). WiRE software (version 4.0, Renishaw, UK) was used to operate the spectrometer and remove cosmic ray interference spikes from the Raman spectra.

UV−vis spectroscopy was used to determine the concentration of graphene in dispersion, through the absorption coefficient at 660 nm ($\alpha_{660\,nm}$) of 2305 ± 24 mL mg^{-1} m^{-1}, measured previously in our laboratory for dispersions of GRod in DCE.[42]

Sedimentation Procedure. Sedimentation experiments were performed by adding 9 mL of dispersion to 1 mL of electrolyte solution, where the initial electrolyte concentration was an order of magnitude higher than desired. Dispersions of NG I and NG II were used in the sedimentation experiments, with a single bulk dispersion of each used to prepare the dispersions at different electrolyte concentrations. Bulk dispersions were sonicated for 5 min prior to removal of aliquots in order to ensure uniformity. After preparation, a first UV−vis spectrum was recorded. Further spectra were recorded over a period of a few days. All absorption spectra were recorded *ex situ*. Two to three spectra were recorded at each time point, and the average absorbance was used to determine the graphene concentration. A 2 mm optical path length quartz cell was used for UV−vis measurements. All glassware used in this work was cleaned with piranha solution (3:1 H_2SO_4:H_2O_2). *Corrosive! Extreme care should be taken when using this solution.*

RESULTS AND DISCUSSION

Initial Dispersions. Initially, GRod powder was dispersed in either DCB or DCE, using bath sonication for 30 min. This produced opaque dispersions, which could be seen to sediment out over a period of hours, leaving behind a more homogeneous gray phase. As shown in Figure 1, addition of

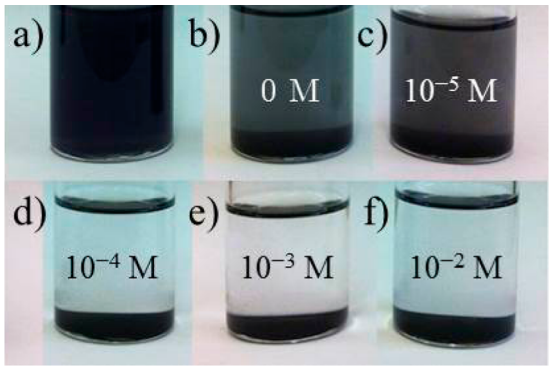

Figure 1. GRod dispersions in DCE, with varying concentrations of BTPPATPBCl electrolyte, at 0 h (a) and 24 h (b−f) after preparation: (a, b) 0, (c) 10^{-5}, (d) 10^{-4}, (e) 10^{-3}, and (f) 10^{-2} M.

the organic electrolyte BTPPATPBCl immediately after dispersion at concentrations of 10^{-4} (d), 10^{-3} (e), and 10^{-2} M (f) resulted in visible sedimentation of all the graphene after 24 h, while 10^{-5} M electrolyte (c) appeared to cause no more sedimentation than in the pure organic solvent. These observations were the same with either DCB or DCE as the dispersing medium. Such behavior is characteristic of an electrostatically stabilized colloid which is destabilized through EDL compression upon addition of electrolyte, with rapid aggregation and sedimentation occurring at the CCC of electrolyte.[23]

At the concentrations used, the majority of BTPPATPBCl dissociates to $BTPPA^+$ and $TPBCl^-$ ions (see Supporting Information, Table S1, for degrees of dissociation). It is assumed that $BTPPA^+$ and $TPBCl^-$ do not directly affect the charge on the graphene surface and instead act as indifferent electrolytes.

UV−vis absorbance spectroscopy was chosen to quantify the effects of electrolyte on dispersion stability, as the concentration of graphene in dispersion is directly related to absorbance through the Beer−Lambert law.[3,19,42] The dispersions were stabilized, in order to have a controlled starting point for the electrolyte induced sedimentation, by removing larger particles/aggregates using the centrifugation procedure described in the Experimental Procedure section. This produced (to the eye) a homogeneous gray dispersion, which gave consistent absorbance readings over a period of several minutes. Additionally, the sonication time was increased to 2 h in order to raise the concentration of dispersed graphene and further break up any macroscopic particles. From this point onward, DCE was used as the sole dispersing solvent. GRod powder was used for initial tests to investigate the effects of electrolyte and determine a suitable range of electrolyte concentrations to study. NG I and NG II powders were used for further detailed study: their differing oxygen contents allowed the effect of differing surface charge to be investigated.

Characterization of Dispersions. XPS spectra of the three graphite powders, along with atomic percentages, are presented in the Supporting Information (Figure S3 and Tables S2, S4, and S6 for GRod, NG I, and NG II, respectively). The C:O ratios (at. %) of GRod, NG I, and NG II were 54.5, 54.1, and 27.1, respectively. Based on the aforementioned work on aqueous GO dispersions[10,28−30] and the prediction of Ameen et al.,[33] it was thought that the greater oxygen content of NG II might produce dispersions with a higher surface charge than dispersions of NG I. ζ values of 52.7 and 53.6 mV were measured for dispersions of NG I and NG II. As ζ measures the charge of the EDL around colloidal particles,[55] the positive sign of these values is consistent with a surface charge generated by negatively charged oxygen-containing functional groups, around which dissociated positive charges form an EDL. However, the similarity in ζ for NG I and NG II, despite their differing oxygen contents, is not consistent with surface charge generation by oxygen-containing functional groups. Additional XPS measurements were performed on the dispersed NG I and NG II flakes (Supporting Information, Tables S5 and S7, respectively) to better characterize the elemental composition of these samples after exfoliation and dispersion. However, significant silicon and oxygen impurities could indicate contamination from glass, from the glassware used to contain dispersions during their preparation by sonication. Therefore, the best guide to the oxygen content of the samples comes from the XPS measurements performed prior to exfoliation, given the additional contamination noted. It is possible that ζ is not an accurate representation of surface charge for these dispersions, as was found by Smith et al.[56] for aqueous dispersions of CNTs, or that the variation in oxygen content between the two graphite powders used here is not sufficient to

DOI: 10.1021/acs.langmuir.5b04219
Langmuir 2015, 31, 13068−13076

significantly affect the surface charging of dispersed particles. Further discussion is present in the Supporting Information.

Complete data and detailed discussion of dispersion characterization by DLS (Figure S4), SEM (Figures S5a and S6), AFM (Figure S5b–d), and Raman spectroscopy (Figures S7–S11) are present in the Supporting Information. Statistics on particle length and height, determined from SEM and AFM, respectively, are presented in Table 1. Briefly, the characterization showed that dispersions of NG I and NG II had very similar lateral particle size distributions, with ca. 90% <1 μm in length and an overall average length of ca. 450 nm. The distribution of particles thicknesses was also quite similar, with ca. 75% of particles were <10 nm/ca. 28 graphene layers thick,[57] though the NG I dispersion contained ca. 10% more particles with thickness >100 nm than the NG II dispersion.

Table 1. Length and Height Statistics of Graphene Particles Dispersed in DCE[a]

dispersion	av length (nm)	<1 μm length (%)	<100 nm height[b] (%)	<10 nm height[b] (%)
GRod	286	97	97	47
NG I	426	93	88	78
NG II	481	89	98	75

[a]Length statistics were determined from SEM and height statistics from AFM. [b]Particle height statistics were based on a limited number of AFM measurements (see Supporting Information, Detailed Experimental Procedure) and are therefore less accurate than the length data.

Stability in Pure Solvent. Initially, graphene dispersions in the absence of electrolyte were monitored over a period of days. Two runs were carried out for dispersions of both NG I and NG II. The average starting concentration of graphite in all dispersions was 31.1 ± 1.7 mg L^{-1} (this includes those with electrolyte, discussed later). Figure 2 shows the concentration profile of NG I and NG II dispersions over time. It is clear that even in the absence of electrolyte, dispersions of NG I and NG II in DCE are not initially stable. For both dispersions, the concentration of graphene dropped significantly after 24 h. However, at times exceeding 24 h, there is clearly a greater concentration of graphene in the NG II dispersion, thus indicating that a greater fraction of this dispersion displays long-term kinetic stability compared to NG I.

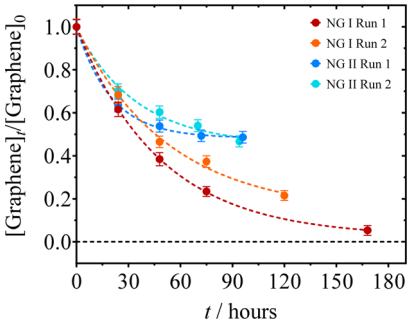

Figure 2. Concentration of graphene at time t, determined from UV–vis absorption and normalized to the initial concentration, as a function of time, for dispersions of NG I and NG II in the absence of electrolyte in DCE. The data have been fitted with eq 2.

The data in Figure 2 were well fitted by single-exponential decays (shown as dashed lines) tending toward a constant value, with the general form shown in eq 2,[58,59] where $[\text{Graphene}]_{\text{unst}}$ is a constant, k is the first-order sedimentation rate constant, and t is time. [Graphene] is the weight concentration of graphene in dispersion, with all concentrations normalized to the concentration at $t = 0$, in order to account for the minor differences in starting concentration. $[\text{Graphene}]_\infty$ is the value toward which the exponential decays converge.

$$\frac{[\text{Graphene}]_t}{[\text{Graphene}]_0} = [\text{Graphene}]_{\text{unst}} e^{-kt} + \frac{[\text{Graphene}]_\infty}{[\text{Graphene}]_0} \quad (2)$$

These fits imply that both dispersions contain an unstable fraction, whose concentration is given by $[\text{Graphene}]_{\text{unst}}$, and a stable fraction, whose concentration is given by $[\text{Graphene}]_\infty$. It should be noted that $[\text{Graphene}]_\infty$ is simply expected to display kinetic stability over time scales significantly longer than those studied here and is not expected to exhibit true thermodynamic stability. Sedimentation rate constants (k), determined from eq 2, are presented in the Supporting Information (Figure S12).

The following values of $[\text{Graphene}]_\infty$ were determined from the exponential fits in Figure 2. NG I: 0.79 ± 0.12 and 4.09 ± 1.19 mg L^{-1} for runs 1 and 2, respectively; NG II: 15.2 ± 0.2 and 14.7 ± 1.4 mg L^{-1} for runs 1 and 2, respectively. These values show that a greater portion of the NG II dispersions, compared to NG I, display long-term kinetic stability. When assessing the characterization of these two dispersions, there are two differentiating factors: the lower oxygen content of NG I (as judged from the pre-exfoliation XPS data) and the greater population of particles with height >100 nm in the NG I dispersion. The greater oxygen content of NG II may lead to a greater particle surface charge in dispersion and, thus, a greater colloidal stability via electrostatic repulsions. However, the differing particle thickness distributions may also contribute to the differing colloidal stabilities.

Note that while the values of $[\text{Graphene}]_\infty$ for the NG II dispersions agree reasonably well, those for dispersions of NG I are quite different. This illustrates the difficulty of reproducing dispersions, even when using aliquots from a single bulk dispersion to prepare all subsequent dispersions.

Onset of Aggregation. To probe the effects of electrolyte on dispersion stability, we have studied dispersion behavior at the onset of aggregation (X_0), which is defined by Forney et al.,[37,39] as the concentration of electrolyte that causes aggregation of 50% of the dispersed material over a given time period. X_0 occurs at lower electrolyte concentrations, and gives information on dispersion stability over longer time scales, than the CCC. Both the CCC and X_0 are quantitative measures of dispersion stability.[37,39] Based on the initial work with GRod dispersions, a range of concentrations from 10^{-8} to 10^{-3} M $\text{BTPPATPBCl}_{(\text{DCE})}$ was chosen for more detailed investigation. These concentrations were selected to provide a large range over which to study the electrolyte effects, while ensuring that the onset of aggregation would be covered. As 24 h was enough for qualitative sedimentation of the GRod dispersions, at sufficient electrolyte concentration, it was chosen as a suitable time frame within which to study X_0.

Plots of the relative graphene concentration after 24 h ($[\text{Graphene}]_{24}/[\text{Graphene}]_0$) vs [BTPPATPBCl] are shown in Figure 3. Dispersions in the absence of electrolyte are also shown for comparison. NG I and NG II displayed similar behavior, with increasing electrolyte concentration initially having little effect upon dispersion stability, until eventually the

DOI: 10.1021/acs.langmuir.5b04219
Langmuir 2015, 31, 13068–13076

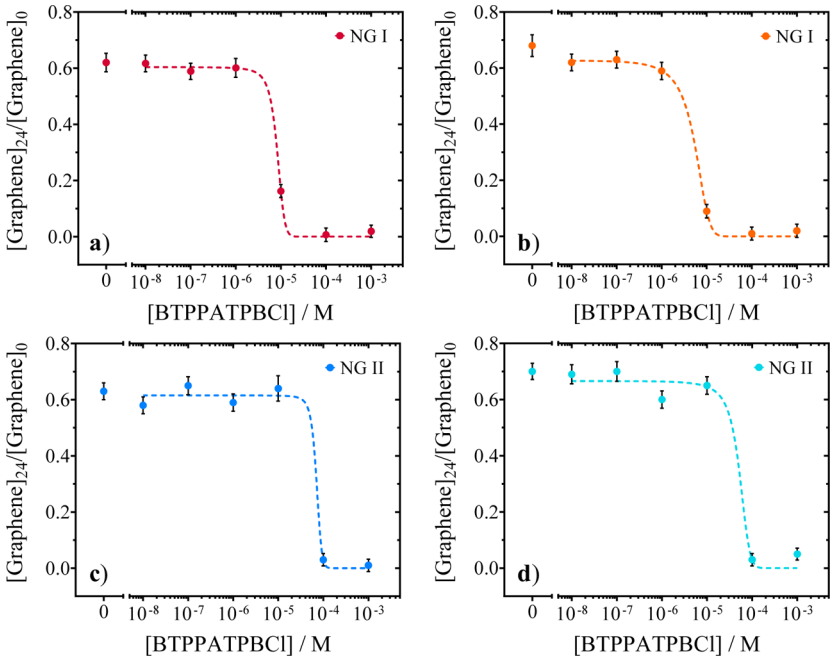

Figure 3. Plots of normalized graphene concentration dispersed in DCE after 24 h of sedimentation vs BTPPATPBCl electrolyte concentration. Electrolyte was added at $t = 0$. (a) NG I, run 1; (b) NG I, run 2; (c) NG II, run 1; (d) NG II, run 2. The plots have been fitted with eq 2 (dashed lines).

dispersion stability decreased markedly. Equation 3 (taken from Ameen et al.,[33] where we have substituted SWCNT for graphene) was used to fit the data in Figure 3 and determine X_0. Equation 3 is an empirical relationship, which approximates the sigmoidal relationship arising from integration of the Maxwell−Boltzmann distribution for energies greater than the EDL barrier.[33] A is the fraction of graphene remaining dispersed at infinite electrolyte dilution, and ΔX is the width of the sigmoidal function.

$$\frac{[\text{Graphene}]_{24}}{[\text{Graphene}]_0} = \frac{A}{1 + e^{[[\text{electrolyte}] - X_0/\Delta X]}} \quad (3)$$

Values of X_0 and A, along with measured values of $[\text{Graphene}]_{24}/[\text{Graphene}]_0$ in the absence of electrolyte, are presented in Table 2. The calculated values of A match up very

Table 2. Actual and Predicted Fractions of Graphene in Dispersion in Pure DCE after 24 h and X_0 Values

dispersion	run	$[\text{Graphene}]_{24}/[\text{Graphene}]_0$ at 0 M	A	X_0 (μM)
NG I	1	0.62 ± 0.03	0.61 ± 0.04	8.27 ± 2.23
	2	0.68 ± 0.04	0.72 ± 0.09	4.96 ± 1.30
NG II	1	0.63 ± 0.03	0.62 ± 0.04	70.6 ± 163
	2	0.70 ± 0.03	0.69 ± 0.12	51.6 ± 34.3

well with the experimental values of $[\text{Graphene}]_{24}/[\text{Graphene}]_0$, which is an important validation and shows that the sigmoidal trends in Figure 3 describe the additional sedimentation resulting from adding electrolyte to the system. Because of the observed sedimentation in the absence of electrolyte, we have adjusted the definition of X_0 here to be the concentration of electrolyte required to sediment 50% of the fraction of graphene dispersed at infinite electrolyte dilution (A). Simply comparing the fractions of graphene dispersed at 10^{-5} M electrolyte illustrates the greater stability of the NG II dispersion, compared with those of NG I, echoing the greater stability of NG II previously observed in the absence of electrolyte. This is borne out in the order of magnitude difference in X_0 between the two dispersions and supports the theory that the extent of electrostatic stabilization is greater for NG II than NG I. There are large errors in the determined X_0 values, particularly for NG II, due to the lack of data points around the center of the sigmoidal curve. In spite of this, the sigmoidal fits are good descriptions of the observed behavior, and analysis of X_0 provides useful information on dispersion stability.

Thus far, we have considered the dispersed graphene particles as charged colloids and interpreted the additional sedimentation caused by electrolyte addition as the result of particle aggregation arising from a compression of the EDL around the dispersed graphene flakes and subsequent reduction in the electrostatic barrier to particle aggregation. It is important to consider alternative explanations for this behavior. Salting out was suggested as the mechanism of electrolyte-induced sedimentation by Ryu et al.,[34] for GO in aqueous dispersion, and Rozhin et al.,[60,61] for CNTs dispersed in NMP. In such a scenario, the addition of electrolyte destabilizes dispersed particles through a combination of reducing the number of solvent molecules able to solvate the particles and increasing the solvophobicity of the particles. First, the concentrations of electrolyte required to destabilize our graphene dispersions are significantly lower than those reported by Ryu et al.[34] and Rozhin et al.[61] Second, the relationship between the concentration of graphene in dispersion and the electrolyte concentration (Figure 3) is well described by a sigmoidal function. This is a classic indicator of DLVO type behavior, whereas the relationship between solvophobicity and electrolyte concentration, derived by Rozhin et al.,[61] was linear.

The additional sedimentation occurring at a certain concentration of electrolyte must then be caused by particle aggregation due to screening of the EDL around the dispersed

DOI: 10.1021/acs.langmuir.5b04219
Langmuir 2015, 31, 13068−13076

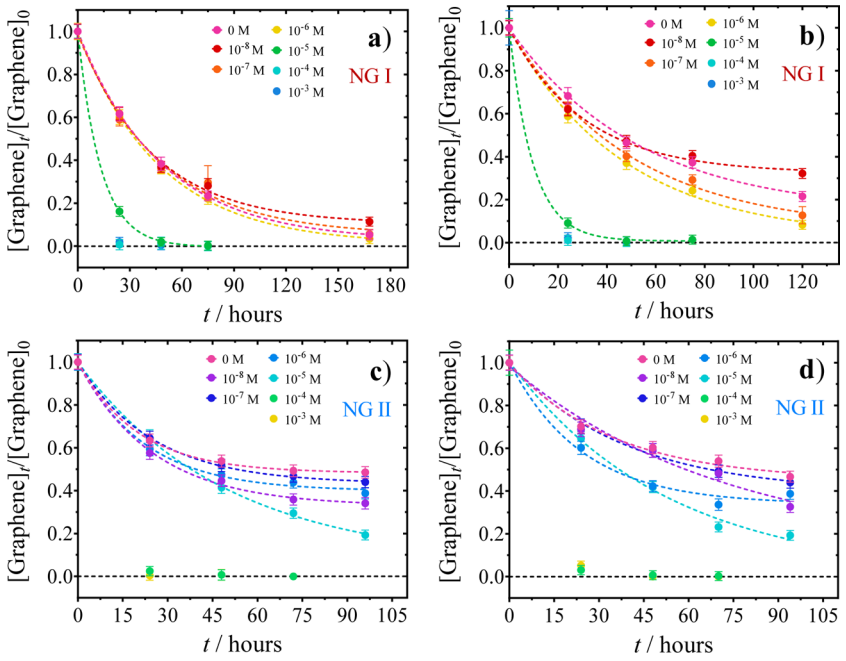

Figure 4. Normalized concentration of graphene dispersed in DCE electrolyte solution at time t plotted against time. (a) NG I, run 1; (b) NG I, run 2; (c) NG II, run 1; (d) NG II, run 2. The data were fitted with the single-exponential decay function, eq 2 (dashed lines).

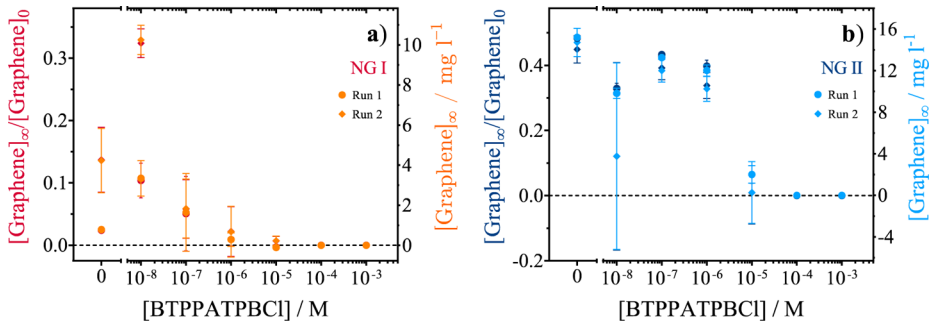

Figure 5. Plots of $[Graphene]_\infty$ vs concentration of BTPPATPBCl, for NG I (a) and NG II (b) dispersed in DCE. The left-hand vertical axis shows $[Graphene]_\infty/[Graphene]_0$, while the right-hand vertical axis shows absolute $[Graphene]_\infty$. These values were determined from the fits in Figure 4, except at 10^{-4} and 10^{-3} M, where they were measured experimentally as zero.

particles and a reduced energetic barrier to particle aggregation. It is therefore likely that the aforementioned greater oxygen content of the NG II particles is the cause of the order of magnitude increase in X_0 for NG II compared to NG I. Though the greater fraction of very thick (>100 nm) particles in the NG I dispersion decrease its colloidal stability compared to NG II (as seen in the dispersions in the absence of electrolyte, Figure 2), variations in particle thickness will have limited effect on particle aggregation, given that face-to-face aggregation is most likely for platelet particles.

Kinetically Stable Dispersion Fraction. The long-term effects of electrolyte on dispersion stability were investigated by monitoring the dispersion concentration over a period of days. Dispersion concentration is plotted against time in Figure 4. As in the absence of electrolyte (Figure 2), all data were well fitted by the single-exponential decay function (eq 2) tending toward $[Graphene]_\infty$. Again, this implies the presence of one stable and one unstable fraction in each dispersion. The rapid sedimentation of dispersions in the two highest electrolyte concentrations (10^{-4} and 10^{-3} M) prevented accurate fitting.

From Figure 4, it appears that the dispersions generally tend toward lower $[Graphene]_\infty$ values as the electrolyte concentration is increased. To better visualize this trend, $[Graphene]_\infty$, determined from the exponential fits in Figure 4, is plotted against electrolyte concentration in Figure 5. With a few exceptions, the $[Graphene]_\infty$ values for both runs are in good agreement with one another for their respective dispersions. However, the errors associated with some of the $[Graphene]_\infty$ values are large, especially for the lowest electrolyte concentration (10^{-8} M), which may be due to the difficulty associated in accurately controlling a low electrolyte concentration.

It is clear from Figure 5 that even the lowest concentrations of electrolyte (10^{-8}–10^{-6} M), which had minimal effect on dispersion stability over 24 h (Figure 3), decrease the fraction of dispersion with long-term kinetic stability. This is presumably the result of a slight decrease in the energetic barrier to particle aggregation, which takes longer than 24 h to manifest. Comparison of $[Graphene]_\infty$ values between NG I and NG II further illustrates the greater stability of the NG II dispersions. Not only does the NG II dispersion contain a larger fraction of dispersion with long-term kinetic stability at each electrolyte concentration, the relative decreases in this

DOI: 10.1021/acs.langmuir.5b04219
Langmuir 2015, 31, 13068−13076

fraction, with each order of magnitude increase in electrolyte concentration, are also lower for the NG II dispersion.

It might be expected that a decreasing electrostatic barrier to aggregation, leading to additional particle aggregation and a decreasing $[\text{Graphene}]_\infty$, would be accompanied by an increase in the sedimentation rate constant, k. However, there was no particular trend in rate constant at electrolyte concentrations below the onset of aggregation, X_0 (Figure S12). It appears that the particle aggregation occurring at electrolyte concentrations an order of magnitude < X_0, which leads to a decreasing $[\text{Graphene}]_\infty$ with increasing electrolyte concentration, is not sufficiently quick to affect the overall rate of sedimentation.

CONCLUSIONS

We have used exfoliation of graphite in DCE to prepare colloidal dispersions of predominantly few-layer graphene. These dispersions contain a fraction of graphene that is unstable and sediments out, leaving behind a kinetically stable graphene fraction. Addition of an indifferent electrolyte was found to destabilize the dispersions, leading to particle aggregation and additional sedimentation, with a sufficient concentration causing complete sedimentation. The relationship between dispersion concentration, after 24 h of sedimentation, and electrolyte concentration was consistent with compression of the EDL around an electrostatically stabilized colloid. The onset of aggregation, X_0, was determined.

Though largely neglected thus far, electrostatic stabilization proved to be an important factor in determining the kinetic stability of nonaqueous graphene dispersions. Further to the previously highlighted thermodynamic criteria of matching the surface energy of graphene and dispersing solvent, when assessing its suitability for dispersing graphene, the study here introduces an additional solvent property to consider from a kinetic viewpoint. Maximizing the relative permittivity of the dispersing solvent should maximize the distance over which electrostatic interactions will permeate and thus maximize the magnitude of the intersheet electrostatic repulsions and dispersion stability.

Two graphene dispersions of similar lateral size and thickness distributions were used in the sedimentation studies. The NG I dispersion was prepared from a graphite source of lower oxygen content than NG II. The more oxidized graphite produced the more stable dispersion, both in terms of the concentration of the kinetically stable fraction and the resistance of the dispersion to electrolyte-induced sedimentation. We hypothesize that this increased stability originates from an increased surface charge on the particles as a result of the greater extent of oxidation. Further studies probing the origin of surface charge in nonaqueous graphene dispersions and its overall importance to the stability of such dispersions would be of great interest.

ASSOCIATED CONTENT

Supporting Information

The Supporting Information is available free of charge on the ACS Publications website at DOI: 10.1021/acs.langmuir.5b04219.

Detailed experimental procedures for DLS, ζ, SEM, and AFM measurements and error calculations; calculation of the degree of BTPPATPBCl dissociation in DCE; XPS data for the graphite powders, GRod, NG I, and NG II and their dispersed flakes, including all atomic percentage values; further discussion of ζ values; hydrodynamic diameters determined from DLS measurements; histograms of particle length, determined from SEM, example SEM images of dispersed graphene flakes, and their discussion; plots of particle height vs particle length, determined from AFM and their discussion; Raman spectra of dispersed graphene flakes and discussion of their features; plots of sedimentation rate constant vs BTPPATPBCl concentration (PDF)

AUTHOR INFORMATION

Corresponding Author

*E-mail: robert.dryfe@manchester.ac.uk (R.A.W.D.).

Notes

The authors declare no competing financial interest.

ACKNOWLEDGMENTS

We thank Amr M. Abdelkader for preparation of graphite powders by ball-milling. We are grateful to the EPSRC (U.K.) funded NEXUS facility (Newcastle University) for performing all XPS experiments and providing advice on analysis of the XPS data. A.N.J.R. thanks EPSRC for award of a PhD studentship. Further support from EPSRC (grants EP/K007033/1 and EP/K016954/1) is also gratefully acknowledged.

REFERENCES

(1) Novoselov, K. S.; Geim, A. K.; Morozov, S. V.; Jiang, D.; Zhang, Y.; Dubonos, S. V.; Grigorieva, I. V.; Firsov, A. A. Electric Field Effect in Atomically Thin Carbon Films. *Science* **2004**, *306*, 666−669.

(2) Novoselov, K. S.; Jiang, D.; Schedin, F.; Booth, T. J.; Khotkevich, V. V.; Morozov, S. V.; Geim, A. K. Two-Dimensional Atomic Crystals. *Proc. Natl. Acad. Sci. U. S. A.* **2005**, *102*, 10451−10453.

(3) Hernandez, Y.; Nicolosi, V.; Lotya, M.; Blighe, F. M.; Sun, Z.; De, S.; McGovern, I. T.; Holland, B.; Byrne, M.; Gun'Ko, Y. K.; et al. High-Yield Production of Graphene by Liquid-Phase Exfoliation of Graphite. *Nat. Nanotechnol.* **2008**, *3*, 563−568.

(4) Novoselov, K. S.; Fal'ko, V. I.; Colombo, L.; Gellert, P. R.; Schwab, M. G.; Kim, K. A Roadmap for Graphene. *Nature* **2012**, *490*, 192−200.

(5) Coleman, J. N. Liquid Exfoliation of Defect-Free Graphene. *Acc. Chem. Res.* **2013**, *46*, 14−22.

(6) Paton, K.; Varrla, E.; Backes, C.; Smith, R.; Coleman, J. N. Scalable Production of Large Quantities of Defect-Free Few-Layer Graphene by Shear Exfoliation in Liquids. *Nat. Mater.* **2014**, *13*, 624−630.

(7) Lotya, M.; Hernandez, Y.; King, P. J.; Smith, R. J.; Nicolosi, V.; Karlsson, L. S.; Blighe, F. M.; De, S.; Wang, Z.; McGovern, I. T.; et al. Liquid Phase Production of Graphene by Exfoliation of Graphite in Surfactant/Water Solutions. *J. Am. Chem. Soc.* **2009**, *131*, 3611−3620.

(8) Lotya, M.; King, P. J.; Khan, U.; De, S.; Coleman, J. N. High-Concentration, Surfactant- Stabilized Graphene Dispersions. *ACS Nano* **2010**, *4*, 3155−3162.

(9) Dikin, D. A.; Stankovich, S.; Zimney, E. J.; Piner, R. D.; Dommett, G. H. B.; Evmenenko, G.; Nguyen, S. T.; Ruoff, R. S. Preparation and Characterization of Graphene Oxide Paper. *Nature* **2007**, *448*, 457−460.

(10) Li, D.; Müller, M. B.; Gilje, S.; Kaner, R. B.; Wallace, G. G. Processable Aqueous Dispersions of Graphene Nanosheets. *Nat. Nanotechnol.* **2008**, *3*, 101−105.

(11) Paredes, J. I.; Villar-Rodil, S.; Martínez-Alonso, A.; Tascón, J. M. D. Graphene Oxide Dispersions in Organic Solvents. *Langmuir* **2008**, *24*, 10560−10564.

(12) Villar-Rodil, S.; Paredes, J. I.; Martínez-Alonso, A.; Tascón, J. M. D. Preparation of Graphene Dispersions and Graphene-Polymer Composites in Organic Media. *J. Mater. Chem.* **2009**, *19*, 3591−3593.

DOI: 10.1021/acs.langmuir.5b04219
Langmuir 2015, 31, 13068−13076

(13) Park, S.; An, J.; Jung, I.; Piner, R. D.; An Jin, S.; Li, X.; Velamakanni, A.; Ruoff, R. S. Colloidal Suspensions of Highly Reduced Graphene Oxide in a Wide Variety of Organic Solvents. *Nano Lett.* **2009**, *9*, 1593−1597.
(14) Ayán-Varela, M.; Paredes, J. I.; Villar-Rodil, S.; Rozada, R.; Martínez-Alonso, A.; Tascón, J. M. D. A Quantitative Analysis of the Dispersion Behavior of Reduced Graphene Oxide in Solvents. *Carbon* **2014**, *75*, 390−400.
(15) Coleman, J. N. Liquid-Phase Exfoliation of Nanotubes and Graphene. *Adv. Funct. Mater.* **2009**, *19*, 3680−3695.
(16) Texter, J. Graphene Dispersions. *Curr. Opin. Colloid Interface Sci.* **2014**, *19*, 163−174.
(17) Verwey, E. J. W.; Overbeek, J. T. G. *Theory of the Stability of Lyophobic Colloids*, 1st ed.; Elsevier Publishsing Company Inc.: New York, 1948.
(18) Khan, U.; Porwal, H.; O'Neill, A.; Nawaz, K.; May, P.; Coleman, J. N. Solvent-Exfoliated Graphene at Extremely High Concentration. *Langmuir* **2011**, *27*, 9077−9082.
(19) Khan, U.; O'Neill, A.; Lotya, M.; De, S.; Coleman, J. N. High-Concentration Solvent Exfoliation of Graphene. *Small* **2010**, *6*, 864−871.
(20) Hamilton, C. E.; Lomeda, J. R.; Sun, Z.; Tour, J. M.; Barron, A. R. High-Yield Organic Dispersions of Unfunctionalized Graphene. *Nano Lett.* **2009**, *9*, 3460−3462.
(21) Hernandez, Y.; Lotya, M.; Rickard, D.; Bergin, S. D.; Coleman, J. N. Measurement of Multicomponent Solubility Parameters for Graphene Facilitates Solvent Discovery. *Langmuir* **2010**, *26*, 3208−3213.
(22) Israelachvili, J. N. *Intermolecular and Surface Forces*, 2nd ed.; Academic Press: London, 1991.
(23) Hunter, R. J. *Introduction to Modern Colloid Science*; Oxford University Press: Oxford, 2002.
(24) Shih, C.-J.; Lin, S.; Strano, M. S.; Blankschtein, D. Understanding the Stabilization of Liquid-Phase-Exfoliated Graphene in Polar Solvents: Molecular Dynamics Simulations and Kinetic Theory of Colloid Aggregation. *J. Am. Chem. Soc.* **2010**, *132*, 14638−14648.
(25) Fu, C.; Yang, X. Molecular Simulation of Interfacial Mechanics for Solvent Exfoliation of Graphene from Graphite. *Carbon* **2013**, *55*, 350−360.
(26) Liu, W. W.; Wang, J. N.; Wang, X. X. Charging of Unfunctionalized Graphene in Organic Solvents. *Nanoscale* **2012**, *4*, 425−428.
(27) Behabtu, N.; Lomeda, J. R.; Green, M. J.; Higginbotham, A. L.; Sinitskii, A.; Kosynkin, D. V.; Tsentalovich, D.; Parra-Vasquez, A. N. G.; Schmidt, J.; Kesselman, E.; et al. Spontaneous High-Concentration Dispersions and Liquid Crystals of Graphene. *Nat. Nanotechnol.* **2010**, *5*, 406−411.
(28) Hong, B. J.; Compton, O. C.; An, Z.; Eryazici, I.; Nguyen, S. T. Successful Stabilization of Graphene Oxide in Electrolyte Solutions: Enhancement of Biofunctionalization and Cellular Uptake. *ACS Nano* **2012**, *6*, 63−73.
(29) Wu, L.; Liu, L.; Gao, B.; Muñoz-Carpena, R.; Zhang, M.; Chen, H.; Zhou, Z.; Wang, H. Aggregation Kinetics of Graphene Oxides in Aqueous Solutions: Experiments, Mechanisms, and Modeling. *Langmuir* **2013**, *29*, 15174−15181.
(30) Szabó, T.; Tombácz, E.; Illés, E.; Dékány, I. Enhanced Acidity and pH-Dependent Surface Charge Characterization of Successively Oxidized Graphite Oxides. *Carbon* **2006**, *44*, 537−545.
(31) Hasan, S. A.; Rigueur, K. J. L.; Harl, R. R.; Krejci, A. J.; Gonzalo-juan, I.; Rogers, B. R.; Dickerson, J. H. Transferable Graphene Oxide Films with Tunable Microstructures. *ACS Nano* **2010**, *4*, 7367−7372.
(32) Cote, L. J.; Kim, F.; Huang, J. Langmuir-Blodgett Assembly of Graphite Oxide Single Layers. *J. Am. Chem. Soc.* **2009**, *131*, 1043−1049.
(33) Ameen, A. A.; Giordano, A. N.; Alston, J. R.; Forney, M. W.; Herring, N. P.; Kobayashi, S.; Ridlen, S. G.; Subaran, S. S.; Younts, T. J.; Poler, J. C. Aggregation Kinetics of Single-Walled Carbon Nanotubes Investigated Using Mechanically Wrapped Multinuclear Complexes: Probing the Tube-Tube Repulsive Barrier. *Phys. Chem. Chem. Phys.* **2014**, *16*, 5855−5865.
(34) Ryu, S.; Lee, B.; Hong, S.; Jin, S.; Park, S.; Hong, S. H.; Lee, H. Salting-Out as a Scalable, in-Series Purification Method of Graphene Oxides from Microsheets to Quantum Dots. *Carbon* **2013**, *63*, 45−53.
(35) Chowdhury, I.; Duch, M. C.; Mansukhani, N. D.; Hersam, M. C.; Bouchard, D. Colloidal Properties and Stability of Graphene Oxide Nanomaterials in the Aquatic Environment. *Environ. Sci. Technol.* **2013**, *47*, 6288−6296.
(36) Wang, H.; Hu, Y. H. Electrolyte-Induced Precipitation of Graphene Oxide in Its Aqueous Solution. *J. Colloid Interface Sci.* **2013**, *391*, 21−27.
(37) Forney, M. W.; Anderson, J. S.; Ameen, A. L.; Poler, J. C. Aggregation Kinetics of Single-Walled Carbon Nanotubes in Non-aqueous Solvents: Critical Coagulation Concentrations and Transient Dispersion Stability. *J. Phys. Chem. C* **2011**, *115*, 23267−23272.
(38) Giordano, A. N.; Chaturvedi, H.; Poler, J. C. Critical Coagulation Concentrations for Carbon Nanotubes in Nonaqueous Solvent. *J. Phys. Chem. C* **2007**, *111*, 11583−11589.
(39) Forney, M. W.; Poler, J. C. Significantly Enhanced Single-Walled Carbon Nanotube Dispersion Stability in Mixed Solvent Systems. *J. Phys. Chem. C* **2011**, *115*, 10531−10536.
(40) Samec, Z. Electrochemistry at the Interface Between Two Immiscible Electrolyte Solutions. *Pure Appl. Chem.* **2004**, *76*, 2147−2180.
(41) Rodgers, A. N. J.; Booth, S. G.; Dryfe, R. A. W. Particle Deposition and Catalysis at the Interface Between Two Immiscible Electrolyte Solutions (ITIES): A Mini-Review. *Electrochem. Commun.* **2014**, *47*, 17−20.
(42) Toth, P. S.; Rodgers, A. N. J.; Rabiu, A. K.; Dryfe, R. A. W. Electrochemical Activity and Metal Deposition Using Few-Layer Graphene and Carbon Nanotubes Assembled at the Liquid-Liquid Interface. *Electrochem. Commun.* **2015**, *50*, 6−10.
(43) Toth, P. S.; Ramasse, Q. M.; Velický, M.; Dryfe, R. A. W. Functionalization of Graphene at the Organic/Water Interface. *Chem. Sci.* **2015**, *6*, 1316−1323.
(44) Warner, J. H.; Ru, M. H.; Gemming, T.; Bu, B.; Briggs, G. A. D. Direct Imaging of Rotational Stacking Faults in Few Layer Graphene. *Nano Lett.* **2009**, *9*, 102−106.
(45) Warner, J. H.; Rümmeli, M. H.; Ge, L.; Gemming, T.; Montanari, B.; Harrison, N. M.; Büchner, B.; Briggs, G. A. D. Structural Transformations in Graphene Studied with High Spatial and Temporal Resolution. *Nat. Nanotechnol.* **2009**, *4*, 500−504.
(46) Hasan, T.; Torrisi, F.; Sun, Z.; Popa, D.; Nicolosi, V.; Privitera, G.; Bonaccorso, F.; Ferrari, A. C. Solution-Phase Exfoliation of Graphite for Ultrafast Photonics. *Phys. Status Solidi B* **2010**, *247*, 2953−2957.
(47) Kim, K. K.; Bae, D. J.; Yang, C.-M.; An, K. H.; Lee, J. Y.; Lee, Y. H. Nanodispersion of Single-Walled Carbon Nanotubes Using Dichloroethane. *J. Nanosci. Nanotechnol.* **2005**, *5*, 1055−1059.
(48) Kim, S.; Yim, J.; Wang, X.; Bradley, D. D. C.; Lee, S.; DeMello, J. C. Spin- and Spray-Deposited Single-Walled Carbon-Nanotube Electrodes for Organic Solar Cells. *Adv. Funct. Mater.* **2010**, *20*, 2310−2316.
(49) Moonoosawmy, K. R.; Kruse, P. To Dope or Not to Dope: The Effect of Sonicating Single-Wall Carbon Nanotubes in Common Laboratory Solvents on Their Electronic Structure. *J. Am. Chem. Soc.* **2008**, *130*, 13417−13424.
(50) Niyogi, S.; Hamon, M. A.; Perea, D. E.; Kang, C. B.; Zhao, B.; Pal, S. K.; Wyant, A. E.; Itkis, M. E.; Haddon, R. C. Ultrasonic Dispersions of Single-Walled Carbon Nanotubes. *J. Phys. Chem. B* **2003**, *107*, 8799−8804.
(51) Korobov, M. V.; Mirakyan, A. L.; Avramenko, N. V.; Smith, A. L.; Ruoff, R. S. Calorimetric Studies of Solvates of C60 and C70 with Aromatic Solvents. *J. Phys. Chem. B* **1999**, *103*, 1339−1346.
(52) Reymond, F. F.; Chopineaux-Courtois, V.; Steyaert, G.; Bouchard, G.; Carrupt, P.-A.; Testa, B.; Girault, H. H. Ionic Partition Diagrams of Ionisable Drugs: pH-Lipophilicity Profiles, Transfer

DOI: 10.1021/acs.langmuir.5b04219
Langmuir 2015, 31, 13068−13076

Mechanisms and Charge Effects on Solvation. *J. Electroanal. Chem.* **1999**, *462*, 235−250.
(53) Cosgrove, T. *Colloid Science: Principles, Methods and Applications*; Blackwell Publishing Ltd.: Oxford, UK, 2005.
(54) Sherwood, J. D.; Stone, H. A. Electrophoresis of a Thin Charged Disk. *Phys. Fluids* **1995**, *7*, 697−705.
(55) Atkins, P.; de Paula, J. *Atkins' Physical Chemistry*, 9th ed.; Oxford University Press: Oxford, 2010.
(56) Smith, B.; Wepasnick, K. Colloidal Properties of Aqueous Suspensions of Acid-Treated, Multi-Walled Carbon Nanotubes. *Environ. Sci. Technol.* **2009**, *43*, 819−825.
(57) Gupta, A.; Chen, G.; Joshi, P.; Tadigadapa, S.; Eklund, P. C. Raman Scattering from High-Frequency Phonons in Supported N-Graphene Layer Films. *Nano Lett.* **2006**, *6*, 2667−2673.
(58) O'Neill, A.; Khan, U.; Nirmalraj, P. N.; Boland, J.; Coleman, J. N. Graphene Dispersion and Exfoliation in Low Boiling Point Solvents. *J. Phys. Chem. C* **2011**, *115*, 5422−5428.
(59) Nicolosi, V.; Vrbanic, D.; Mrzel, A.; McCauley, J.; O'Flaherty, S.; Mcguinness, C.; Compagnini, G.; Mihailovic, D.; Blau, W. J.; Coleman, J. N. Solubility of M06S4.5I4.5 Nanowires in Common Solvents: A Sedimentation Study. *J. Phys. Chem. B* **2005**, *109*, 7124−7133.
(60) Fedorov, M. V.; Arif, R. N.; Frolov, A. I.; Kolar, M.; Romanova, A. O.; Rozhin, A. G. Salting out in Organic Solvents: A New Route to Carbon Nanotube Bundle Engineering. *Phys. Chem. Chem. Phys.* **2011**, *13*, 12399−12402.
(61) Frolov, A. I.; Arif, R. N.; Kolar, M.; Romanova, A. O.; Fedorov, M. V.; Rozhin, A. G. Molecular Mechanisms of Salt Effects on Carbon Nanotube Dispersions in an Organic Solvent (N-Methyl-2-Pyrrolidone). *Chem. Sci.* **2012**, *3*, 541.

DOI: 10.1021/acs.langmuir.5b04219
Langmuir 2015, 31, 13068−13076